

Pauli spin blockade in carbon nanotube double quantum dots

M. R. Buitelaar,¹ J. Fransson,² A. L. Cantone,¹ C. G. Smith,¹ D. Anderson,¹ G. A. C. Jones,¹ A. Ardavan,³ A. N. Khlobystov,⁴ A. A. R. Watt,⁴ K. Porfyrikis,⁴ and G. A. D. Briggs⁴

¹*Cavendish Laboratory, University of Cambridge, Cambridge, CB3 0HE, United Kingdom*

²*Department of Physics and Materials Science, Uppsala University, 751 21 Uppsala, Sweden*

³*Clarendon Laboratory, Oxford University, Oxford OX1 3PU, United Kingdom*

⁴*Department of Materials, Oxford University, Oxford OX1 3PH, United Kingdom*

(Received 11 February 2008; published 25 June 2008)

We report Pauli spin blockade in a carbon nanotube double quantum dot defined by tunnel barriers at the contacts and a structural defect in the nanotube. We observe a pronounced current suppression for negative source-drain bias voltages, which is investigated for both symmetric and asymmetric coupling of the quantum dots to the leads. The measured differential conductance agrees well with a theoretical model of a double quantum dot system in the spin-blockade regime, which allows us to estimate the occupation probabilities of the relevant singlet and triplet states. This work shows that effective spin-to-charge conversion in nanotube quantum dots is feasible and opens the possibility of single-spin readout in a material that is not limited by hyperfine interaction with nuclear spins.

DOI: [10.1103/PhysRevB.77.245439](https://doi.org/10.1103/PhysRevB.77.245439)

PACS number(s): 73.63.Fg, 73.23.Hk, 73.63.Kv, 85.35.Kt

I. INTRODUCTION

The electron spin is a natural two-level system and therefore is attractive as a quantum bit in quantum information processing schemes. Spin qubits defined in quantum dots are of particular interest because of the possibility to isolate, manipulate, and measure single spins.¹ Much of the attraction of spin qubits in quantum dots is also related to the relatively long time over which a superposition of opposite spin states of a single electron remains coherent. This long spin coherence time is a direct result of the electron's small magnetic moment, which ensures it couples only weakly to its environment. The inevitable problem this poses for the readout of a single spin is elegantly overcome in double quantum dot systems by converting the spin information to a charge state using the phenomenon of Pauli spin blockade, which occurs when certain transitions between two quantum dots are forbidden by spin selection rules^{2,3} as illustrated in Fig. 1. Significant experimental effort on spin qubits defined

in quantum dots in GaAs/AlGaAs heterostructures has already resulted in the demonstration of driven coherent oscillations of single electron spins⁴ and the coherent exchange of two electron spins in a square-root-of-swap quantum operation.⁵

While significant as a proof of principle that single spin manipulation and readout in a solid-state environment are feasible, these experiments also demonstrated that the spin coherence time in these devices is limited by hyperfine interactions with the Ga and As nuclei.⁴⁻⁷ As a result, the number of coherent single-spin rotations that can presently be observed within the spin coherence time in GaAs-based quantum dots is several orders of magnitude below the typical figure of merit of 10^4 quantum operations for a fault tolerant quantum computer.

There is therefore a strong incentive to develop spin qubits in materials in which hyperfine interactions are much reduced or absent altogether. Carbon-based materials such as carbon nanotubes or graphene are excellent candidates in this

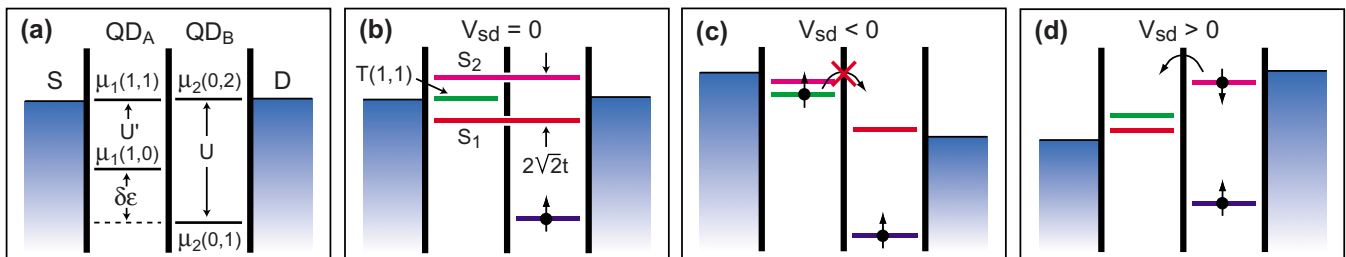


FIG. 1. (Color online) (a) Schematics of the electrochemical potentials of the relevant one- and two-electron states of a double quantum dot in the absence of a tunnel coupling between them. The level offset between the single-particle states on both dots is given by $\delta\epsilon$. The on-site charging energy and electrostatic coupling energy are shown as U and U' , respectively. (b) When the tunnel coupling t between the quantum dots is significant, the $S(1,1)$ and $S(0,2)$ singlet states hybridize to form molecular bonding (S_1) and antibonding (S_2) singlet states, which separate from the $T(1,1)$ triplet states. (c) When a negative bias voltage is applied and one of the $T(1,1)$ triplet states becomes occupied, the $(1,1) \rightarrow (0,2)$ transition is not allowed because, by virtue of the Pauli principle, the $(0,2)$ state has to be a spin singlet, and any further current flow is blocked. (d) For opposite bias conditions the $(0,2) \rightarrow (1,1)$ transition through the singlet states is allowed. Note that for finite detuning, the S_1 and S_2 singlet states (as well as the triplet states) are still extended molecular states but are dominated by the $(0,2)$ and $(1,1)$ charge states in the way indicated by the schematics.

respect. Due to the absence of hyperfine coupling in the dominant ^{12}C isotope, the spin coherence times are expected to be very long,^{8,9} while the recent observation of spin-orbit interaction in nanotube quantum dots suggests the possibility of electrical control of the spin states.^{9–12} In this work, we show that spin blockade is readily observed in weakly coupled carbon nanotube quantum dots even for many electrons on the nanotube and for temperatures of order one Kelvin. We therefore conclude that effective spin-to-charge conversion in carbon nanotube quantum dots is feasible and that single-spin manipulation and readout in nanotubes is a promising and realistic prospect.

II. NANOTUBE DEVICES

The device we consider consists of an individual carbon nanotube filled with Sc@C_{82} molecules (that is a Sc atom inside a C_{82} cage) contacted by electron-beam defined palladium source (S) and drain (D) electrodes that are separated by 300 nm. The degenerately doped Si/SiO₂ substrate (300 nm oxide) is used as back gate. The study of carbon nanotubes filled with Sc@C_{82} is motivated by the long spin coherence times of the unpaired spins on the encapsulated Sc atoms as observed by us in ensemble measurements.¹³

Measurements on twelve different devices suggest that even though the presence of Sc@C_{82} may lead to observable band structure modification or charge transfer (doping) between the nanotubes and Sc@C_{82} , the low-temperature transport properties are remarkably similar to those of empty nanotubes.¹⁴ These findings are consistent with recent transport experiments on nanotubes with encapsulated C_{60} molecules,^{15,16} as well as with recent density functional theory calculations of spin interactions of chains of Sc@C_{82} inside carbon nanotubes.¹⁷ The conclusions of our present work will therefore apply equally well to empty carbon nanotubes.

III. RESULTS AND DISCUSSION

The linear-response conductance of the device as a function of gate voltage measured at temperature $T=1.4$ K is shown in Fig. 2(b), which displays a series of irregular conductance peaks. A variation in peak height and spacing is common for carbon nanotube quantum dots and is generally attributed to scattering by defects along the nanotube. As demonstrated by a combination of scanning probe and transport experiments,¹⁸ structural defects in particular lead to resonant electron scattering in which the defects can be transparent or opaque depending on the electrochemical potential (and hence the gate voltage). Defects could be introduced in our nanotubes by, for example, the acid treatment used to purify the samples from magnetic impurities. However, defects are also commonly observed in as-grown nanotubes such as those made by chemical vapor deposition and for which typical scattering lengths of ~ 150 nm were reported.¹⁸ Low-temperature transport experiments on a number of our nanotube devices of the geometry studied here indicate that most consist of a series of (two or three) quantum dots.

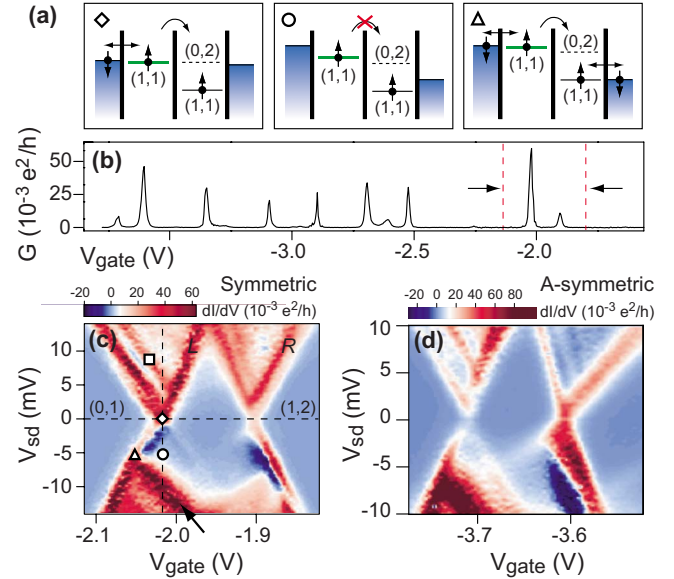


FIG. 2. (Color online) (a) Schematic level diagrams for different transport regimes corresponding to the measurements of panel (c), see symbols. (b) Linear-response conductance of the device measured at $T=1.4$ K. (c) Color-scale plot of the differential conductance (dI/dV) as a function of source-drain bias voltage (V_{sd}) and gate voltage (V_g) for the gate region indicated by the arrows in panel (b). Dark blue corresponds to negative dI/dV . The ordered pairs (n, m) indicate the effective electron occupancy in each quantum dot. (d) Differential conductance for a different region of V_g , showing a pronounced asymmetry in both bias and gate voltage.

Double quantum dots in carbon nanotubes in which the tunnel barrier between the dots is due to a defect in the nanotube are relatively common and have been studied previously in, e.g., Refs. 19 and 20. Typically, a double quantum dot is identified by the characteristic honeycomb pattern that develops as two independent gate electrodes (each coupled to a different quantum dot) are varied.²¹ In our device we only have the ability to vary a single gate electrode (the back gate). Nevertheless, a detailed understanding of the physical phenomena underlying the electronic transport properties can be obtained by studying the differential conductance (dI/dV) as a function of gate (V_g) and bias voltage (V_{sd}), as demonstrated for double quantum dots by Ono *et al.*² Here we focus on two pairs of peaks around $V_g = -1.95$ V and $V_g = -3.65$ V of which the differential conductance is shown in Figs. 2(c) and 2(d), respectively. The most striking feature of the dI/dV plots is the pronounced asymmetry in the bias voltage and the current suppression and appearance of negative differential conductance for negative V_{sd} (dark blue regions). Also note that while Fig. 2(c) is approximately symmetric in gate voltage, this symmetry is clearly broken in Fig. 2(d).

The lack of periodicity in the linear-response conductance, the pronounced negative differential conductance, as well as the striking difference in the slopes of adjacent Coulomb diamonds [most apparent in Fig. 2(d)] are clearly at odds with a model of a single quantum dot. As we will show below, these features can be explained well by invoking Pauli spin blockade in a double quantum dot. The simplest

model of two coupled single-level quantum dots as introduced in Fig. 1 suffices to explain our measurements. This might seem surprising given that the nanotubes will contain many electrons, but it is justified by the large single-electron level spacing ΔE (see below) and the simple even-odd shell filling of carbon nanotube quantum dots.²² Recent work on GaAs double dot systems containing more than two electrons (up to ~ 10) could also be explained in terms of effective single-level quantum dots.^{23,24}

A. Double quantum dot Hamiltonian

To quantitatively compare the measurements in Fig. 2 with an interpretation in terms of spin blockade, we have used a many-body density matrix approach to calculate the current and population numbers of the eigenstates of two coupled single-level quantum dots. The double quantum dot (DQD) and the leads are modeled by the Hamiltonian $\mathcal{H} = \mathcal{H}_L + \mathcal{H}_R + \mathcal{H}_{\text{DQD}} + \mathcal{H}_T$, where $\mathcal{H}_{L(R)}$ models the left (right) lead in a free electronlike approximation. The double quantum dot is modeled by

$$\begin{aligned} \mathcal{H}_{\text{DQD}} = & \sum_{n=A,B} \left(\sum_{\sigma} \varepsilon_{n\sigma} d_{n\sigma}^{\dagger} d_{n\sigma} + U n_{n\uparrow} n_{n\downarrow} \right) \\ & + U' (n_{A\uparrow} + n_{A\downarrow}) (n_{B\uparrow} + n_{B\downarrow}) \\ & + \sum_{\sigma} (t d_{A\sigma}^{\dagger} d_{B\sigma} + \text{H.c.}). \end{aligned} \quad (1)$$

In the model we have two levels, $\varepsilon_{A\sigma}$ and $\varepsilon_{B\sigma}$, where $\sigma = \uparrow, \downarrow$ is the electron spin. Here, $d_{A(B)\sigma}^{\dagger}$ ($d_{A(B)\sigma}$) creates (annihilates) an electron in quantum dot $A(B)$ with spin σ . The on-site Coulomb charging energy and electrostatic coupling energy are denoted by U and U' , respectively, whereas t is the tunneling rate between the quantum dots (see also Fig. 1). The last term in \mathcal{H} accounts for the tunneling between the leads and the DQD. This model neglects spin-orbit and hyperfine interactions.

The Hamiltonian \mathcal{H}_{DQD} is transformed into diagonal form, e.g., $\mathcal{H}_{\text{DQD}} = \sum_{Nn} E_{Nn} |N, n\rangle \langle N, n|$, where E_{Nn} is the energy for the eigenstate $|N, n\rangle$ with N electrons, where n is a state label (in our model there are 16 eigenstates, such that $N=0, n=1, N=1, n=1, \dots, 4, N=2, n=1, \dots, 6, N=3, n=1, \dots, 4, N=4, n=1$). This enables a many-body density matrix approach for calculating the population number probabilities P_{Nn} of the corresponding state $|N, n\rangle$, to the first-order approximation with respect to the coupling $\Gamma^{L(R)}$ to the left (right) lead. This order of approximation is based on that only the diagonal transitions $|N, n\rangle \rightarrow |N, n\rangle$ are included, while effects from off-diagonal transitions such as $|N, n\rangle \rightarrow |N, n'\rangle$ would require a higher order expansion of the rate equations for the population number probabilities. Our calculation provides the dynamics of the population numbers as a function of the bias voltage and equilibrium electrochemical potential. Knowledge of the population number probabilities enables the calculation of the current and differential conductance through the system, using standard techniques. The approach provides complete knowledge of the matrix elements $\langle N, n | \mathcal{H}_T | N \pm 1, m \rangle$ for transitions between states differing in electron number by one. This information allows

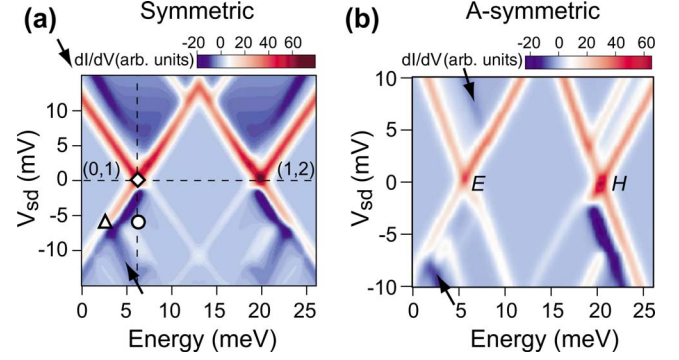


FIG. 3. (Color online) (a) Color-scale plot of the calculated differential conductance as a function of source-drain bias voltage and gate voltage. The model parameters used are $\delta\epsilon=5$ meV, $U'=12$ meV, $U=17$ meV, (both quantum dots) and $t=0.7$ meV. The relative voltage drop over the tunnel barrier between the two quantum dots is $\Delta V_{\text{QD}}/V_{sd} \sim 0.15$. The temperature is set to $T=4$ K. The symbols correspond to the schematics in Fig. 2. (b) Same as panel (a) for asymmetric coupling of the double quantum dot to the leads as described in the main text.

for detailed analysis of which states are involved in the conductance and of which state(s) are responsible for spin and Coulomb blockade. The method is more thoroughly described in Ref. 3.

B. Double quantum dot model parameters

We start by comparing the model predictions with the measurements of Fig. 2(c). In the model, and in the analysis below, we assume that the charging energy U and the capacitive coupling to the gate electrode is the same for both quantum dots. This approximation is justified by the symmetry (in V_g) of the data in Fig. 2(c). The result of the model calculations using an appropriate set of parameters, which we will discuss below, is shown in Fig. 3(a). The calculated differential conductance is in good agreement with the experimental data of Fig. 2(c) for the low bias regime while differences are observed at higher bias voltages. Figure 4 illustrates how the differential conductance [evaluated in Fig. 4 for the electrochemical potential corresponding to the dotted vertical line in Fig. 3(a)] is related to the occupation probabilities of the various one- and two-electron states. These calculations also show [see Fig. 4(b)] that the observed current suppression for negative V_{sd} is indeed the result of a near unity occupation probability of the $T(1,1)$ triplet states.

The first model parameter to consider is the voltage drop ΔV_{QD} over the tunnel barrier between the two quantum dots in the presence of a source-drain bias voltage. The relative voltage drop can be obtained from the slopes of the diamonds in the experimental data, marked by L and R in Fig. 2(c), and from an electrostatic model of the device,^{21,25} and yields $\Delta V_{\text{QD}}/V_{sd} \sim 0.15$. As a result, the bias voltage V_{sd} acts as a knob that effectively controls the level offset $\delta\epsilon$ (or “detuning”) between the quantum dots.²¹ The magnitude of $\delta\epsilon$ can be extracted from the excitation line indicated by the triangle in Figs. 2(c) and 3(a). The position of the triangle in the dI/dV plots corresponds to the situation in which (ne-

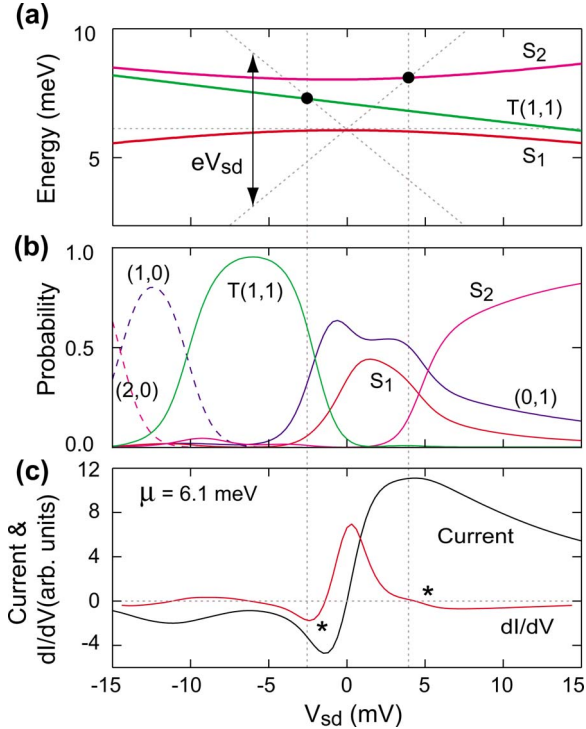


FIG. 4. (Color online) (a) The current and dI/dV can be understood from the evolution of the two singlet states [S_1 (red) and S_2 (magenta)] and the triplet states (green) as a function of V_{sd} . The model parameters used here correspond to the situation of Fig. 3(a). The diagonal lines indicate the opening of the bias window as V_{sd} is increased. The electrochemical potential $\mu = 6.1$ meV corresponds to the dotted vertical line in Fig. 3(a). (b) Calculated occupation probabilities for the various one- and two-electron states as a function of V_{sd} . (c) Peaks in the current and dI/dV are observed when transitions between the one-electron and two-electron states are energetically accessible.

glecting the tunnel coupling) the electrochemical potentials on the left and right quantum dot are aligned with the electrochemical potentials of the source and drains electrodes, respectively [see right schematic in Fig. 2(a)]. Taking into account the voltage drop between the quantum dots, this yields $\delta\epsilon \sim 5$ meV. When the bias voltage is increased beyond this point, the model calculation shows [see Fig. 4(b)] that the double dot gets trapped in a $(1,0)$ charge state [this excitation line is indicated by the lower arrow in Fig. 3(a)]. As a result, the current *decreases* again with increasing V_{sd} . In the experiment, however, this is not observed. This difference can be understood considering that the model does not account for inelastic scattering processes. This approach is justified in the spin blockade regime since relaxation due to, e.g., electron-phonon interaction is strongly suppressed if the transition involves a spin flip.²⁶ On the other hand, the $(1,0) \rightarrow (0,1)$ transition does not require a spin flip, and energy relaxation by phonon emission will be effective in the experiment. As a result, an *increase* in current is expected (and indeed observed) along this excitation line, as indicated by the arrow in Fig. 2(c).

A similar reasoning would explain the absence of negative dI/dV that is observed in the model for positive V_{sd} . For

example, the excitation line observed in the experiment [Fig. 2(c), square, and upper arrow in Fig. 3(a)] could be due to a transition between the S_2 and S_1 states, which does not require a spin flip either. However, since the observed excitation line is exactly parallel to the ground state transition, we tentatively attribute it to a single-dot excitation, which yields $\Delta E \sim 4$ meV. If we assume the conventional nanotube dispersion relation, the level spacing is related to the nanotube length L through $\Delta E = \hbar v_F / 4L$, where \hbar is Planck's constant, and $v_F = 8.1 \times 10^5$ m/s is the Fermi velocity.²⁷ For $\Delta E \sim 4$ meV this yields $L = 200$ nm, which given the source-drain separation of 300 nm, would imply two quantum dots of similar size.

The electrostatic coupling energy U' can be obtained from the size of the main diamond (positive half) in Fig. 2(c) from which we obtain $U' \sim 10$ – 15 meV.²¹ The charging energy on the individual quantum dots is more difficult to determine exactly. The most satisfactory correspondence between the data and model is obtained for $U \sim 17$ meV for both quantum dots, consistent with dot lengths of order ~ 100 – 200 nm.²² We verified that the conclusions of our work are not sensitive to the exact value of U .

The ratio of the tunnel coupling to the level offset is crucial for the observation of spin blockade, and $t/\delta\epsilon \ll 1$ must be satisfied for it to be clearly observed.³ To appreciate this, consider that a current flow in the double dot involves transitions between the one-electron state and the two-electron singlet or triplet states. The one-electron state is a superposition of the $(0,1)$ and $(1,0)$ charge states, i.e., of the kind $\alpha|0,1\rangle + \beta|1,0\rangle$, and the probability of finding the electron in the energetically excited $(1,0)$ state depends directly on $t/\delta\epsilon$.²¹ Because in the spin blockade regime, transferring an electron to the drain electrode involves a transition from a triplet state to the $(1,0)$ charge state; a current flow will be strongly suppressed if $\beta \ll \alpha$. Note that this is not the case for a current mediated by the singlet states, which follows the sequence $(1,1) \rightarrow (0,2) \rightarrow (0,1) \rightarrow (1,1)$.

In our experiments, the tunnel coupling can be extracted from the small leakage current of ~ 100 pA that is observed in the spin blockade regime [see Fig. 5(a)]. As compared to the ~ 5 nA measured at positive V_{sd} , this implies a current suppression of a factor of ~ 50 . Given the previous estimate for $\delta\epsilon$ of approximately 5 meV, the model requires $t < 0.7$ meV to provide a similar suppression factor. The observed leakage current also directly puts a lower bound of $e/I \sim 2$ ns on the spin relaxation time T_1 in carbon nanotube quantum dots. Note however that this is likely to be a strong underestimate of the intrinsic spin-flip relaxation time in carbon nanotubes and that the observed leakage current can be fully accounted for by transitions mediated by the remaining finite occupation probabilities of the one-electron and two-electron singlet states. The strong dependence of the leakage current on the tunnel coupling is illustrated in Fig. 5(b).

C. Asymmetric coupling to the leads

While the measurements of Fig. 2(c) are approximately symmetric in gate voltage, this is not the case for the differential conductance shown in Fig. 2(d). As compared to the

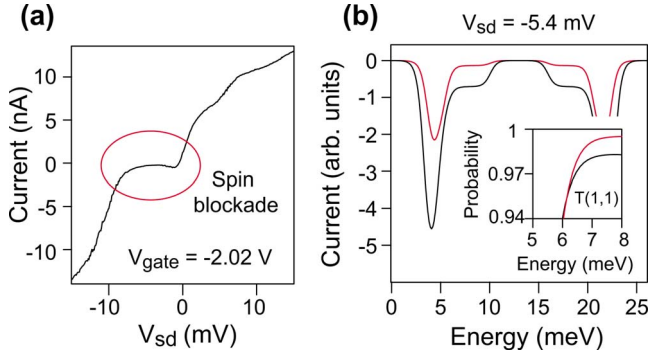


FIG. 5. (Color online) (a) Measured current as a function of V_{sd} at gate voltage $V_g = -2.02$ V, corresponding to the dotted vertical line in Fig. 2(c). The red oval indicates the regime of Pauli spin blockade with measured leakage current of ~ 100 pA. (b) Calculated current traces as a function of electrochemical potential at $V_{sd} = -5.4$ mV for the model parameters of Fig. 3(a). The tunnel couplings are $t = 0.7$ meV (black) and $t = 0.3$ meV (red). Inset: maximum occupation probability of the triplet states.

symmetric situation, there is a pronounced tilt in the slopes of the Coulomb diamonds, and a strong negative differential conductance is observed only along the right edge of the Coulomb diamond. In the model these features are reproduced by introducing an asymmetry in the potential drop at the source and drain electrodes and in the tunnel couplings Γ_s/Γ_d of the leads to the quantum dots while keeping other parameters such as U , U' , and $\delta\epsilon$ identical to the symmetric situation. The tunnel coupling is set to $t = 1.2$ meV. The result for $\Delta V_s/\Delta V_d = 3/2$ and $\Gamma_s/\Gamma_d = 1/5$ is shown in Fig. 3(b), which corresponds well with the experimental data [see Fig. 2(d)].

The dependence of the current in the Pauli spin blockade regime on the asymmetry in the tunnel couplings for the model used here is described in detail in Ref. 3. An intuitive way to understand the effect of the asymmetry on the triplet occupation probability (and therefore on the leakage current) is the following: in the spin blockade regime as considered above, an electron has a high probability to enter the double dot from the source electrode to form a $T(1,1)$ triplet state but a low probability to exit to the drain (hence the high occupation probability). An asymmetric coupling $\Gamma_s \ll \Gamma_d$, on the other hand, has the precise opposite effect. The result is a reduction in the triplet occupation probability such that negative differential conductance is not observed along the edge of the Coulomb diamond in the left part of Fig. 3(b).

The strong negative differential conductance along the Coulomb diamond edge on the right side of Fig. 3(b) can be understood considering the (broken) electron-hole symmetry of the double dot. Whereas the linear-response conductance at point E in Fig. 3(b) corresponds to an electron moving from the source to the drain electrode, the conductance at point H corresponds to a hole moving in the opposite direction.²¹ While the asymmetry in the tunnel rates (partially) lifts the spin blockade for the electron cycle, it

enhances the blockade for the hole cycle (as it moves in the opposite direction). The result is a strong $T(1,1)$ triplet occupation probability and negative differential conductance in the dI/dV plots.

Note that several of the excitation lines in the model (indicated by the arrows) are also observed in the data. The difference in the polarity of the excitation (negative versus positive dI/dV in the model and experiment, respectively) is attributed to energy relaxation by, e.g., phonon emission, which is not accounted for in the model. As discussed above, inelastic scattering will be effective in the experiment for transitions that do not require a spin-flip.

IV. CONCLUSIONS AND OUTLOOK

In conclusion, we present measurements of the differential conductance of a carbon nanotube double quantum dot showing Pauli spin blockade. The measurements are well described by a theoretical model of the device, which allows us to estimate the relevant singlet and triplet occupation probabilities of the double quantum dot. Since the phenomena of spin blockade enables spin-to-charge conversion in quantum dots, our findings present an important step toward single-spin readout and spin qubit operations in carbon-based devices that are not limited by hyperfine interactions. An additional advantage of nanotubes in this respect is the large energy scales observed here, which compare favorably to other systems such as lateral GaAs or Si double quantum dots. In electron-spin resonance experiments,⁴ which are limited by photon-assisted tunneling, this would allow considerably larger oscillating fields and hence much faster single-spin rotations. In fact, the significantly larger g factor of carbon nanotubes ($g \approx 2$) as compared to GaAs devices ($g \approx -0.44$) would already provide a fivefold gain.

For future experiments, control of the individual quantum dots and the tunnel coupling is imperative. Fully tunable carbon nanotube quantum dots have already been studied by a number of groups, but spin blockade had not been previously observed.^{19,20,28–30} This seems surprising given the clear signatures seen here at a relatively high temperature of 1.4 K. This difference is likely to be related to the condition $t/\delta\epsilon \ll 1$, which must be satisfied for the observation of spin blockade in double quantum dots. As our device is rather small (dot sizes of order 100–200 nm) and does not make use of metal top gates that would add to the overall device capacitance, most quantum dot energy scales are nearly an order of magnitude larger than in Refs. 19, 20, 28, and 29. We expect that when the device dimensions and/or the tunnel couplings are sufficiently reduced, spin blockade will also be observed in top-gated carbon nanotube quantum dots.

ACKNOWLEDGMENTS

We thank John Jefferson, John Morton, and Karl Petersson for discussions and Hisanori Shinohara for assistance with the production of the fullerene material. This research is part of QIP IRC (GR/S82176/01).

- ¹D. Loss and D. P. DiVincenzo, *Phys. Rev. A* **57**, 120 (1998).
- ²K. Ono, D. G. Austing, Y. Tokura, and S. Tarucha, *Science* **297**, 1313 (2002).
- ³J. Fransson and M. Råsaender, *Phys. Rev. B* **73**, 205333 (2006).
- ⁴F. H. L. Koppens, C. Buizert, K. J. Tielrooij, I. T. Vink, K. C. Nowack, T. Meunier, L. P. Kouwenhoven, and L. M. K. Vandersypen, *Nature (London)* **442**, 766 (2006).
- ⁵J. R. Petta, A. C. Johnson, J. M. Taylor, E. A. Laird, A. Yacoby, M. D. Lukin, C. M. Marcus, M. P. Hanson, and A. C. Gossard, *Science* **309**, 2180 (2005).
- ⁶A. C. Johnson, J. R. Petta, J. M. Taylor, A. Yacoby, M. D. Lukin, C. M. Marcus, M. P. Hanson, and A. C. Gossard, *Nature (London)* **435**, 925 (2005).
- ⁷F. H. L. Koppens, J. A. Folk, J. M. Elzerman, R. Hanson, L. H. Willems van Beveren, I. T. Vink, H. P. Tranitz, W. Wegscheider, L. P. Kouwenhoven, and L. M. K. Vandersypen, *Science* **309**, 1346 (2005).
- ⁸Y. G. Semenov, K. W. Kim, and G. J. Iafrate, *Phys. Rev. B* **75**, 045429 (2007).
- ⁹D. V. Bulaev, B. Trauzettel, and D. Loss, *Phys. Rev. B* **77**, 235301 (2008).
- ¹⁰T. Ando, *J. Phys. Soc. Jpn.* **69**, 1757 (2000).
- ¹¹D. Huertas-Hernando, F. Guinea, and A. Brataas, *Phys. Rev. B* **74**, 155426 (2006).
- ¹²F. Kuemmeth, S. Ilani, D. C. Ralph, and P. L. McEuen, *Nature (London)* **452**, 448 (2008).
- ¹³G. W. Morley, B. J. Herbert, S. M. Lee, K. Porfyrakis, T. J. S. Dennis, D. Nguyen-Manh, R. Scipioni, J. van Tol, A. P. Horsfield, A. Ardavan, D. G. Pettifor, J. C. Green, and G. A. D. Briggs, *Nanotechnology* **16**, 2469 (2005).
- ¹⁴Depending on the coupling of the Sc@C₈₂ filled carbon nanotubes to the leads, we have observed Coulomb blockade, Kondo and Fano features.
- ¹⁵P. Utko, J. Nygård, M. Monthieux, and L. Noé, *Appl. Phys. Lett.* **89**, 233118 (2006).
- ¹⁶C. H. L. Quay, J. Cumings, S. J. Gamble, A. Yazdani, H. Kataura, and D. Goldhaber-Gordon, *Phys. Rev. B* **76**, 073404 (2007).
- ¹⁷L. Ge, B. Montanari, J. H. Jefferson, D. G. Pettifor, N. M. Harrison, and G. A. D. Briggs, arXiv:0710.3061 (unpublished).
- ¹⁸M. Bockrath, W. Liang, D. Bozovic, J. H. Hafner, C. M. Lieber, M. Tinkham, and H. Park, *Science* **291**, 283 (2001).
- ¹⁹N. Mason, M. J. Biercuk, and C. M. Marcus, *Science* **303**, 655 (2004).
- ²⁰H. I. Jørgensen, K. Grove-Rasmussen, K.-Y. Wang, A. M. Blackburn, K. Flensberg, P. E. Lindelof, and D. A. Williams, arXiv:0711.3245 (unpublished).
- ²¹W. G. van der Wiel, S. De Franceschi, J. M. Elzerman, T. Fujisawa, S. Tarucha, and L. P. Kouwenhoven, *Rev. Mod. Phys.* **75**, 1 (2003).
- ²²D. H. Cobden, M. Bockrath, P. L. McEuen, A. G. Rinzler, and R. E. Smalley, *Phys. Rev. Lett.* **81**, 681 (1998).
- ²³H. W. Liu, T. Fujisawa, T. Hayashi, and Y. Hirayama, *Phys. Rev. B* **72**, 161305(R) (2005).
- ²⁴A. C. Johnson, J. R. Petta, C. M. Marcus, M. P. Hanson, and A. C. Gossard, *Phys. Rev. B* **72**, 165308 (2005).
- ²⁵Assuming that the charging energies U for the two quantum dots are identical and that the gate capacitance (C_g) of the quantum dots is small as compared to the capacitances of the quantum dots to the source (C_s) and drain (C_d) electrodes, as well as the mutual capacitance (C_m), the relative voltage drop is given by $\Delta V_{\text{QD}}/V_{sd} \sim (U-U')/(U+U')$. From the same model we obtain $C_s=C_d \sim 4.9$ aF, $C_m \sim 13.3$ aF, and $C_g \sim 0.6$ aF.
- ²⁶T. Fujisawa, D. G. Austing, Y. Tokura, Y. Hirayama, and S. Tarucha, *Nature (London)* **419**, 278 (2002).
- ²⁷Here we assume that the subband degeneracy is broken, which will generally be the case when atomic defects are present.
- ²⁸M. R. Gräber, W. A. Coish, C. Hoffmann, M. Weiss, J. Furer, S. Oberholzer, D. Loss, and C. Schönberger, *Phys. Rev. B* **74**, 075427 (2006).
- ²⁹H. I. Jørgensen, K. Grove-Rasmussen, J. R. Hauptmann, and P. E. Lindelof, *Appl. Phys. Lett.* **89**, 232113 (2006).
- ³⁰S. Sapmaz, C. Meyer, P. Beliczynski, P. Jarillo-Herrero, and L. P. Kouwenhoven, *Nano Lett.* **6**, 1350 (2006).